CHALMERS
UNIVERSITY OF TECHNOLOGY

Joint Tx-Rx Beamforming for Optimal Gain and Self-Interference Mitigation in In-Band Full-Duplex Arrays: Theory, Figures of Merit, and

Downloaded from: https://research.chalmers.se, 2025-09-25 04:03 UTC

Citation for the original published paper (version of record):
Ayebe, M., Maaskant, R., Gunnarsson, S. et al (2025). Joint Tx-Rx Beamforming for Optimal Gain and Self-Interference Mitigation in In-Band
Full-Duplex Arrays: Theory, Figures of Merit, and Validation. IEEE Antennas and Wireless Propagation Letters, 24(6): 1317-1321. http://dx.doi.org/10.1109/LAWP.2025.3534882

N.B. When citing this work, cite the original published paper.

© 2025 IEEE. Personal use of this material is permitted. Permission from IEEE must be obtained for all other uses, in any current or future media, including reprinting/republishing this material for advertising or promotional purposes, or reuse of any copyrighted component of this work in other works.

(article starts on next page)

Joint Tx-Rx Beamforming for Optimal Gain and Self-Interference Mitigation in In-Band Full-Duplex Arrays: Theory, Figures of Merit, and Validation

Mustafa Ayebe, Rob Maaskant, Sten E. Gunnarson, Johan Malmström, Marianna Ivashina, and Henrik Holter

***Abstract*—We introduce a novel joint transmit (Tx) and receive (Rx) beamforming method and relevant performance metrics for in-band full-duplex (IBFD) antenna systems, addressing two major challenges: self-interference (SI) leakage from the transmitter to the receiver and non-linear gain compression in the receiver's low-noise amplifiers (LNAs). Conventional methods treat Tx and Rx beamforming separately, often failing to balance SI suppression with sufficient Tx gain. In contrast, our approach achieves two key objectives. First, it maximizes Tx array antenna gain while ensuring that SI at the LNA input remains below a predefined threshold, preventing saturation and maintaining linearity. Second, it suppresses residual SI at the receiver output, improving the signal-to-SI ratio by effectively separating the desired signal from residual interference. This method is validated using a commercial RF system-on-chip evaluation board and 3×5 Tx and Rx Vivaldi antenna arrays operating in the 3–6 GHz band. Experimental results show that the conventional Tx maxGain beamformer achieves approximately 22 dB isolation between closely spaced Tx and Rx arrays. In contrast, the proposed Tx beamforming method provides over 45 dB isolation, with a Tx array gain of up to 10 dBi. Overall, the joint Tx-Rx beamforming method achieves more than 80 dB isolation with a 10 dBi Rx array gain for the IBFD system, representing a significant improvement over conventional methods.**

***Index Terms*—antenna array, beamforming, interference suppression, in-band full-duplex, and RFSoC.**

I. Introduction

In-band full-duplex (IBFD) technology enables simultaneous transmission and reception on the same frequency, potentially doubling spectral efficiency and data rates. This is beneficial for applications such as increasing base station capacity through concurrent uplink/downlink in next-generation cellular networks, enabling real-time updates in automotive radars, and continuous target tracking in surveillance systems [1]–[3]. However, the main challenge in IBFD is managing self-interference (SI), where transmitted signals leak into the receiver, especially when Tx and Rx antennas are in close proximity, as in compact base stations or onboard vehicles [4]. This challenge is exacerbated by dynamic range limitations, where strong SI from the transmitter reduces the receiver's ability to detect weak signals [5], [6]. Additionally, hardware imperfections, such as non-linearity of power amplifiers (PAs) and impedance mismatch in analog circuitry, further distort the transmitted signal, complicating SI cancellation (SIC).

Analog and digital SIC methods are necessary to overcome these challenges. Analog SIC uses devices like couplers, circulators, or hybrids for signal isolation between Tx and Rx [7], achieving moderate SIC (20-30 dB) due to bandwidth limits and insertion loss. Despite this, analog SIC remains crucial for reducing dynamic range demands and aiding digital SIC algorithms, such as maximum ratio combining (MRC) [8], signal-to-noise-plus-interference ratio (SNIR) [9], and recursive least-square (RLS) adaptive filtering. These algorithms use accurate channel models to optimize Rx beamformer weights, achieving up to 100 dB SIC in simulations and 30-40 dB in experiments [10]. However, residual SI (10-20 dBc) remains with changing frequency- and direction-dependent effects. Non-linearity compensation techniques [11], using the PA output as a reference signal, show SIC of 40-50 dB with residuals typically below 10 dBc. However, they are limited by specificity to certain non-linearity types and may not align well with joint Tx-Rx beamforming adjustments, leading to suboptimal SIC and compromised antenna pattern and gain.

Our recent work in [12] has extended a conventional Tx beamforming algorithm that maximizes antenna gain to mitigate SI-induced nonlinear gain compression in the receiver low-noise amplifiers (LNAs). This approach enables controlling SI on the Rx side, laying the foundation for effective IBFD operation. However, [12] primarily focused on static SI conditions, where SI effects are direction-independent, and did not address the need for integrated Tx-Rx design. In this paper, we propose a joint Tx-Rx optimal beamforming method that combines SIC capabilities on both sides while adapting them during beam-steering. The extended Tx beamformer keeps SI from Tx-Rx coupling below a predefined threshold, controlling SI at the LNA inputs to prevent saturation while maximizing Tx antenna gain. On the Rx side, a conventional MRC beamformer is modified to suppress residual SI at the receiver output, maintaining a high SNIR by effectively separating the desired signal from SI. The novel contributions include a generalized model of IBFD systems with joint beamforming and figures of merit that can guide isolation requirements at the element/array level, ensuring optimal performance without overdesigning individual components. Experimental validation using a state-of-the-art RFSoC ZCU216 and arrays of strongly coupled antenna elements demonstrates the performance gains of this method, practical measurement procedure, and real-time processing capabilities.

Mustafa Ayebe, Rob Maaskant, and Marianna Ivashina are with the Antenna Systems Group, Dept. of Electrical Engineering, Chalmers University of Technology. Sten E. Gunnarson and Johan Malmström are with Surveillance, Saab. Henrik Holter with Hardware Research, Ericsson AB.

This work, conducted within the Advanced Digitalization program at the WiTECH Centre [DIGIARRAY project], is financed by VINNOVA, Ericsson, Saab, Satcube, and Chalmers.

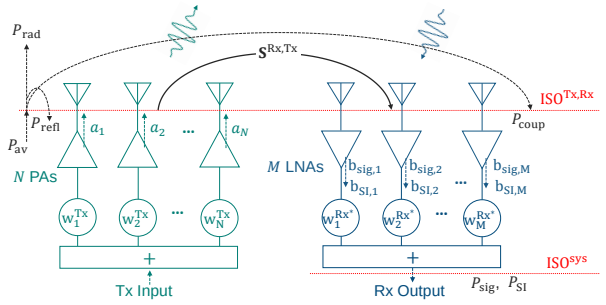

Fig. 1: IBFD system model with separate-aperture Tx and Rx array antennas. For the Tx antenna, the incident power a-waves are defined at the PA outputs. The received power b-waves are defined at the LNA outputs of the Rx antenna and include both the desired received signal (blue incident wave) and the residual SI resulting from the mutual coupling between the Tx and Rx chains of the system.

II. In-Band Full-Duplex Antenna System Model

Fig. 1 shows the IBFD system model with N-element Tx and M-element Rx antenna arrays where the elements are connected to their corresponding amplifiers and beamformers. The Tx beamforming vector $\mathbf{w}^{\text{Tx}}$ optimizes the element excitation across the Tx array, while the Rx beamforming vector $(\mathbf{w}^{\text{Rx}})^*$ optimizes the Rx element weights. Using the power wave definitions [13], the incident power waves at the PAs output are represented by $\mathbf{a} = [a_1, a_2, \ldots, a_N]^{\text{T}}$, and in the linear region of the PAs, $\mathbf{a} \propto \mathbf{w}^{\text{Tx}}$, enabling coherent beamforming. The outgoing power wave vector after the LNAs, $\mathbf{b}_{\text{sig}}$ is the desired signal, and $\mathbf{b}_{\text{SI}}$ is the residual SI due to IBFD operation.

The available power at the Tx antenna ports P_{av}, coupled power at the Rx antenna ports P_{coup}, total desired received signal and residual SI power at the Rx beamformer port P_{sig} and P_{SI}, and radiated power P_{rad} are defined as follows:

$$
\begin{aligned}
&P_{\text{av}} = \frac{1}{2}\mathbf{a}^{\text{H}}\mathbf{a}, \quad P_{\text{coup}} = \frac{1}{2}\mathbf{a}^{\text{H}}\left(\mathbf{S}^{\text{Rx,Tx}}\right)^{\text{H}}\mathbf{S}^{\text{Rx,Tx}}\mathbf{a},\\
&P_{\text{sig}} = \frac{1}{2}\left|\left(\mathbf{w}^{\text{Rx}}\right)^{\text{H}}\mathbf{b}_{\text{sig}}\right|^2, \quad P_{\text{SI}} = \frac{1}{2}\left|\left(\mathbf{w}^{\text{Rx}}\right)^{\text{H}}\mathbf{b}_{\text{SI}}\right|^2,\\
&P_{\text{rad}} = \frac{1}{2\eta}\mathbf{a}^{\text{H}}\mathbf{G}^{\text{H}}\mathbf{G}\mathbf{a}, \quad \mathbf{G} = [\boldsymbol{G}_1, \boldsymbol{G}_2, \ldots, \boldsymbol{G}_N],
\end{aligned} \tag{1}
$$

Here, $\mathbf{S}^{\text{Rx,Tx}}$ is the mutual coupling matrix, $(.)^{\text{H}}$ denotes the Hermitian operator, and $\mathbf{b}_{\text{SI}} = S_{21}^{\text{LNA}}\mathbf{S}^{\text{Rx,Tx}}\mathbf{a}$, where S_{21}^{LNA} is the LNA voltage gain. η is the characteristic impedance of free space, and $\mathbf{G}$ is a column-augmented matrix, where $\boldsymbol{G}_n$ is the complex far-field nth embedded element pattern (EEP). In this formulation, we assume that the system operates in an SI-dominated regime, with noise neglected.

We consider the problem of quantifying the system isolation from joint Tx and Rx beamforming. First, the **Rx array antenna isolation** at the LNAs input when the Tx array elements are excited with $\mathbf{w}^{\text{Tx}}$ can be defined as:

$$
\text{ISO}^{\text{Tx,Rx}}(\mathbf{w}^{\text{Tx}}) = \frac{P_{\text{av}}(\mathbf{w}^{\text{Tx}})}{P_{\text{coup}}(\mathbf{w}^{\text{Tx}})} = \frac{\mathbf{a}^{\text{H}}\mathbf{a}}{\mathbf{a}^{\text{H}}\left(\mathbf{S}^{\text{Rx,Tx}}\right)^{\text{H}}\mathbf{S}^{\text{Rx,Tx}}\mathbf{a}} \tag{2}
$$

When monitoring the m-th receiving element, with all Tx elements excited by $\mathbf{w}^{\text{Tx}}$, the coupled power is given by $P_{\text{coup}} = P_{\text{coup},m} = \frac{1}{2}\mathbf{a}^{\text{H}}\left(\boldsymbol{S}_m^{\text{Rx,Tx}}\right)^{\text{H}}\boldsymbol{S}_m^{\text{Rx,Tx}}\mathbf{a}$ so $\text{ISO}^{\text{Tx,Rx}}(\mathbf{w}^{\text{Tx}})$ reduces to the **Rx element isolation** $\text{ISO}_m^{\text{Tx,Rx}}$.

Finally, for the joint Tx-Rx beamforming, the **total IBFD system isolation** at the Rx beamformer port is:

$$
\text{ISO}^{\text{sys}} = \frac{P_{\text{av}}(\mathbf{w}^{\text{Tx}})}{P_{\text{SI}}(\mathbf{w}^{\text{Tx}}, \mathbf{w}^{\text{Rx}})} = \frac{\mathbf{a}^{\text{H}}\mathbf{a}}{\left|\left(\mathbf{w}^{\text{Rx}}\right)^{\text{H}} S_{21}^{\text{LNA}}\mathbf{S}^{\text{Rx,Tx}}\mathbf{a}\right|^2} \tag{3}
$$

The element isolation will always exceed the array isolation since P_{coup} sums the coupled powers at individual element ports (*see the proof* App. A). This principle guides adjusting isolation requirements to slightly exceed the minimum possible element isolation, hence ensuring optimal performance without overdesigning the system.

III. Proposed Beamforming Method

Tx Beamforming: The proposed Tx beamforming algorithm uses prior knowledge of $\mathbf{S}^{\text{Rx,Tx}}$, estimated via a digital SI channel, to optimize beamformer weights in a desired direction. While it follows a *conventional Tx maximum gain beamformer* [14], its novelty lies in maintaining the Rx array antenna isolation above a specified level, $\kappa^{\text{Tx,Rx}}$. This threshold, defined as the ratio of P_{av} to the LNA's 1 dB compression point with modulation-induced backoff, prevents saturation and preserves linear operation. The algorithm operates as follows (see [12] for more details):

$$
\begin{aligned}
\max_{\mathbf{w}^{\text{Tx}}} \quad & 4\pi\frac{P_{\text{rad}}(\mathbf{w}^{\text{Tx}})}{P_{\text{av}}(\mathbf{w}^{\text{Tx}})}\\
\text{subject to} \quad & \text{ISO}^{\text{Tx,Rx}}(\mathbf{w}^{\text{Tx}}) \geq \kappa^{\text{Tx,Rx}}
\end{aligned} \tag{4}
$$

After finding $\mathbf{w}_{\text{opt}}^{\text{Tx}}$, one could check the resultant minimum element isolation, $\min(\text{ISO}_m^{\text{Tx,Rx}})$ and, if it is significantly larger than the required isolation for preventing saturation, iteratively relax the threshold until the $\min(\text{ISO}_m^{\text{Tx,Rx}})$ is just above the requirement (see numerical results in Sec. IV-B).

Rx Beamforming: The optimal Rx weight vector $(\mathbf{w}^{\text{Rx}})^*$ maximizes the desired signal power, as in a *conventional Rx MRC beamformer*, while it also ensures the total SI power below a set level κ_{SI} (e.g. the receiver noise floor), i.e.,

$$
\begin{aligned}
\max_{\mathbf{w}^{\text{Rx}}} \quad & P_{\text{sig}}(\mathbf{w}^{\text{Rx}})\\
\text{subject to} \quad & P_{\text{SI}}(\mathbf{w}^{\text{Rx}}) = \kappa_{\text{SI}} \quad \& \quad (\mathbf{w}^{\text{Rx}})^{\text{H}}\mathbf{w}^{\text{Rx}} = 1
\end{aligned} \tag{5}
$$

IV. Analysis and Validation Results

A. IBFD system case study and measurement setup

Our selected case study of the proposed beamforming method includes an IBFD system with 3×5 Tx and Rx Vivaldi element arrays (3–6 GHz) that are placed side-by-side with electrically small (0.5λ at 6 GHz) separation and, hence, strongly coupled [*see* Fig. 2]. The antenna setup is connected to the Zynq UltraScale+ RFSoC ZCU216 Kit [16], which supports real-time digital signal processing for communication testing, including calibration [17] and IBFD operation. The block diagram of the integrated antenna-RFSoC measurement platform, shown in Fig. 3, integrates ADCs, DACs, programmable logic (PL), and digital processing system (PS) cores. In this setup, no PAs or LNAs are used to simplify the initial validation in the linear regime. The movable probe antenna connects to Amplifier 1 (Amp1) or Amplifier 2

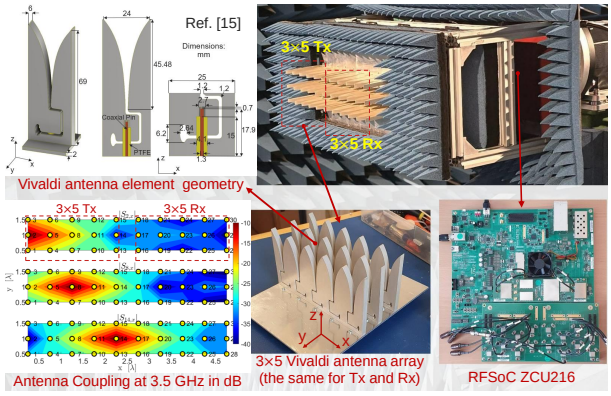

Fig. 2: Case study: An IBFD antenna system with 3×5 Tx and 3×5 Rx Vivaldi arrays, placed side-by-side, installed in an anechoic chamber. The arrays share identical dimensions and element geometry. Each 3D-printed silver-coated element is fed by a coaxial probe through an aluminum ground plane [15].

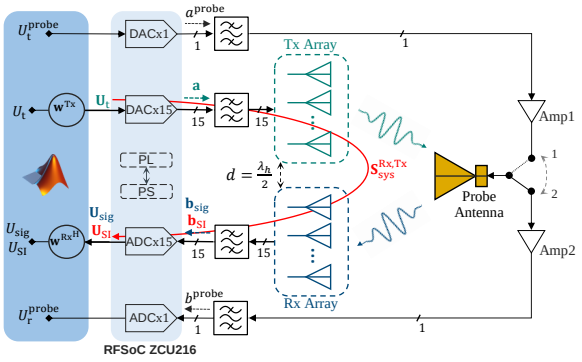

Fig. 3: Block diagram of the integrated IBFD antenna system - RFSoC measurement setup, used for demonstration.

(Amp2) to compensate for signal propagation losses during measurements. A custom-designed PCB [*see* Fig. 2] with commercial off-the-shelf baluns[1] converts unbalanced signals for differential DAC outputs and ADC inputs.

The *digital* continuous waveform at frequency ω_0 is $f[n] = \mathfrak{Re}\{U_t e^{jn\omega_0/f_s}\}$, with $n \in \mathbb{Z}$ and DAC sampling frequency f_s. The complex phasor U_t is multiplied by the beamforming vector $\mathbf{w}^{\text{Tx}}$, forming the 15×1 vector $\mathbf{U}_t$. These signals are converted to phase-synchronized analog waves $\mathbf{a} \propto \mathbf{U}_t$, passed through baluns, and incident to the Tx antennas. The received waves at the Rx array, after baluns, form the 15×1 vectors, $\mathbf{b}_{\text{sig}}$ and $\mathbf{b}_{\text{SI}}$, representing desired and interferer waves, respectively. After being processed by ADCs, the *digital* signal $\mathbf{U}_{\text{sig}} \propto \mathbf{b}_{\text{sig}}$ and SI $\mathbf{U}_{\text{SI}} \propto \mathbf{b}_{\text{SI}}$ are multiplied by $(\mathbf{w}^{\text{Rx}})^{\text{H}}$ to arrive at the post-processed complex phasor amplitude U_{sig} and U_{SI}. We use MATLAB to control the board, generate and capture time-domain waveforms, and apply the FFT for frequency-domain analysis. The measurement procedure includes the following steps:

1) A coupling Matrix Measurement: With the probe antenna off, each Tx array element is excited with 1 V while the others remain unexcited. The measured voltages at the Rx array form one column of the coupling matrix, $\mathbf{S}_{\text{sys}}^{\text{Rx,Tx}}$. It relates Tx and Rx voltages in a linear system: $\mathbf{U}_{\text{SI}} = \mathbf{S}_{\text{sys}}^{\text{Rx,Tx}} \mathbf{U}_{\text{t}}$.

[1]Product No: X4BD40L1-50100G

2) Tx EEP Measurements: The probe antenna is connected to an Amp2 via switch position 2. Each Tx element is excited with a 1 V signal while the others remain unexcited. The received voltage $U_{\text{r}}^{\text{probe}}$ is proportional to the Tx EEP.

3) Rx EEP Measurements: Through switch position 1, the probe antenna acts as the transmitter and $U_{\text{t}}^{\text{probe}}$ is set to 1 V. The measured voltages at the Rx elements are proportional to the EEPs of the Rx antennas.

4) Beamformer Optimization: The Tx array antenna EEPs and $\mathbf{S}_{\text{sys}}^{\text{Rx,Tx}}$ are used to optimize $\mathbf{w}^{\text{Tx}}$ in (4). We assumed that $\mathbf{S}^{\text{Rx,Tx}} = \mathbf{S}_{\text{sys}}^{\text{Rx,Tx}}$ and $\mathbf{a} = \mathbf{U}_{\text{t}}$ (proportionality constants cancel in the power ratios). Then, $(\mathbf{w}^{\text{Rx}})^*$ is optimized in (5) using the Rx antenna EEPs for the final required SI residual level.

B. Results and Discussion

Figs 4 and 5 exemplify the proposed joint Tx-Rx beamforming method for the above-described IBFD system at $f_0 = 3.5$ GHz. Fig. 4(a) shows the Tx array gain vs. Rx array isolation trade-off by comparing various isolation thresholds. The case where $\text{ISO}^{\text{Tx,Rx}} > 30$ dB demonstrates an optimal solution, achieving approximately 20 dB higher isolation with minimal gain loss compared to the conventional Tx maximum gain beamformer. Fig.4(b) reveals that the achieved element isolation surpasses array isolation by 10–20 dB, depending on element position and beamsteering angle. To avoid overdesign, it is useful to bring $\min(\text{ISO}_m^{\text{Tx,Rx}})$ closer to the $\kappa^{\text{Tx,Rx}}$, which dictates linearity requirements. This can be realized by adjusting the isolation threshold through numerical iterations. For instance, in Fig. 4(c), $\kappa^{\text{Tx,Rx}} = 30$ dB is met after two iterations when $\text{ISO}^{\text{Tx,Rx}} > 18$ dB, resulting in $\min(\text{ISO}_m^{\text{Tx,Rx}}) = 35.9$ dB. Finally, Rx beamforming further suppresses SI below $\kappa_{\text{SI}} = -80$ dBW at the Rx output. Fig. 4(d) compares Rx array gain and IBFD system isolation for Rx MRC and the proposed Rx beamformer when the Tx maxGain beamformer applied to Tx array. The eigenvalue spectrum, calculated from both simulated and measured Tx-Rx coupling matrices (shown in Fig. 5(a)), provides insight into the available degrees of freedom for optimizing $\mathbf{w}^{\text{Tx}}$. This is determined by the number of eigenvectors corresponding to dominant eigenvalues above a chosen threshold of $\kappa^{\text{Tx,Rx}} = 45$ dB[2]. As expected, the agreement between the simulated and measured lower eigenvalues (associated with stronger coupling) is very good and reduces for higher eigenvalues (i.e., weaker coupling). The Rx element isolation between antenna ports changes after connecting the beamforming circuit, altering antenna loading. The change in element isolation was under 4 dB for 50 ± 10 Ω loading. Figs. 5(b) and (c) indicate that the conventional Tx maxGain beamformer achieves 17–27 dB Rx array isolation, whereas the proposed beamformer exceeds 45 dB. Minor isolation variations due to $\pm 4^\circ$ phase errors in $\mathbf{w}^{\text{Tx}}$ are observed in Fig. 5(b), increasing with higher isolation requirements but remaining within acceptable limits, as shown in Fig. 5(c). Fig. 5(d) shows a generally good agreement between the simulated and measured antenna gains. The observed reduction of the Tx antenna gain at large negative angles (e.g., 4.5 dB at -30°) compared to the conventional Tx maxGain beamformer

[2]$\kappa^{\text{Tx,Rx}} = 45$ dB corresponds to max. $P_{\text{av}} \approx 12$ dBm, so LNA's 1 dB compression point with modulation-induced backoff ≈ -33 dBm.

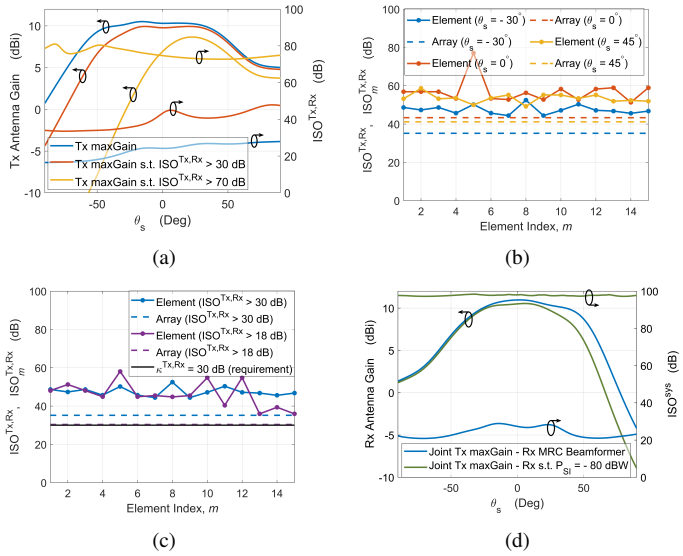

Fig. 4: Simulated; (a) Tx antenna gain and Rx array isolation for the conventional and proposed Tx beamformers; (b) Rx array/elements isolation for the proposed Tx beamformer (for $\text{ISO}^{\text{Tx,Rx}} > 30$ dB) at different E-plane scan angles; (c) Rx array/elements isolation under different isolation constraints at $\theta_s = -30°$; and (d) Rx array gain and IBFD system isolation for Rx MRC vs. the proposed Rx beamformer when Tx maxGain is applied.

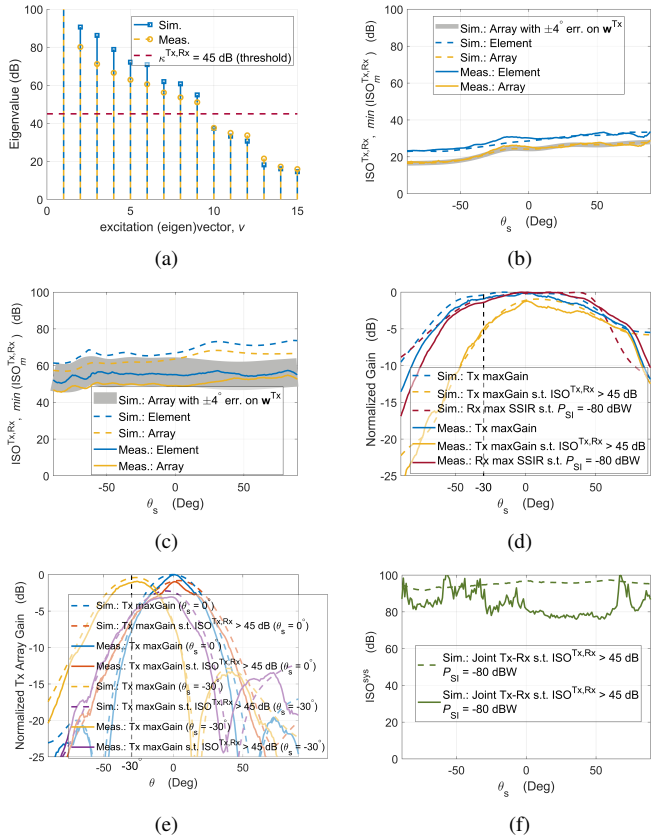

Fig. 5: Simulation-measurement comparison: (a) The eigenvalue spectrum of $[(\mathbf{S}_{\text{sys}}^{\text{Rx,Tx}})^{\text{H}}\mathbf{S}_{\text{sys}}^{\text{Rx,Tx}}]^{-1}$; (b) The Rx array/element isolation for the conventional Tx maxGain beamformer; (c) The Rx array/element isolation for the proposed Tx beamformer when $\kappa^{\text{Tx,Rx}} = 45$ dB; (d) The Tx and Rx antenna gains for the proposed join Tx-Rx beamformer with $\kappa^{\text{Tx,Rx}} = 45$ dB and $\kappa_{\text{SI}} = -80$ dBW (practical RFSoC ZCU216 noise floor level); (e) Normalized the Tx array radiation pattern at different E-plane scan angles; and (f) The total IBFD system isolation with proposed joint Tx - Rx beamformer.

is attributed to the limited number of usable excitation vectors meeting the isolation requirement. The relative difference for the Rx array gain at large negative angles is mainly due to the absorber effects and at large positive angles due to interference. Similarly, Fig. 5(e) shows Tx radiation patterns widening in the proposed method compared to conventional Tx maxGain beamformer due to a reduced number of excitation vectors. Lastly, Fig. 5(f) demonstrates total IBFD system isolation surpassing 80 dB with joint Tx-Rx beamforming. Minor degradation in measurements likely stems from phase errors in RFSoC DAC/ADC outputs and dynamic range limitations. Although the proposed joint Tx-Rx beamforming approach maintains strong isolation across frequencies, with performance decreasing away from the center, this study specifically focuses on a narrowband scenario.

V. Conclusion

The joint Tx-Rx beamforming method for IBFD systems balances SI suppression with optimal antenna gain. By dynamically adjusting beamforming weights, it significantly improves system isolation, as validated by experiments. Future work includes scaling to broader frequency bands, integrating PAs/LNAs, and addressing non-linear regimes.

Appendix A
Proof on Minimum ISO for Subspace Beamformer

Let define $f(\mathbf{z}) = (\mathbf{z}^{\text{H}}\mathbf{A}\mathbf{z})/(\mathbf{z}^{\text{H}}\mathbf{B}\mathbf{z})$, where $\mathbf{A}$ and $\mathbf{B}$ are positive matrices. The extremum of $f(\mathbf{z})$ is found by solving the generalized eigenvalue problem, $\mathbf{A}\mathbf{v}_n = \lambda_n\mathbf{B}\mathbf{v}_n$. Hence, λ_n satisfies $\lambda_n = f(\mathbf{v}_n)$. If $\lambda_1 \geq \lambda_2 \geq \ldots \geq \lambda_P$ and $f(\mathbf{z}) \geq \kappa$, then $\{\lambda_n\}_{n=1}^{K} \geq \kappa$, and we can express $\mathbf{z} = \mathbf{V}\boldsymbol{\alpha}$ where $\mathbf{V} = [\mathbf{v}_1, \ldots, \mathbf{v}_K]$. Therefore, using $\mathbf{A}\mathbf{V} = \mathbf{B}\mathbf{V}\boldsymbol{\Lambda}$, here $\boldsymbol{\Lambda} = \text{diag}(\lambda_1, \ldots, \lambda_K)$, so $f(\mathbf{z})$ can be reformulated as:

$$f(\boldsymbol{\alpha}) = \frac{\boldsymbol{\alpha}^{\text{H}}\mathbf{V}^{\text{H}}\mathbf{B}\mathbf{V}\boldsymbol{\Lambda}\boldsymbol{\alpha}}{\boldsymbol{\alpha}^{\text{H}}\mathbf{V}^{\text{H}}\mathbf{B}\mathbf{V}\boldsymbol{\alpha}} \tag{6}$$

Solving $\nabla_{\boldsymbol{\alpha}^{\text{H}}} f(\boldsymbol{\alpha}) = 0$ yields $\boldsymbol{\Lambda}\boldsymbol{\alpha} = f\boldsymbol{\alpha}$, leading to $(\boldsymbol{\Lambda} - f\mathbf{I})\boldsymbol{\alpha} = 0$. The characteristic equation for non-trivial solutions is: $\prod_{n=1}^{K}(\lambda_n - f) = 0$. Thus, the minimum value of f is $f = \lambda_K \geq \kappa$, proving $\min f(\boldsymbol{\alpha}) = \lambda_K \geq \kappa$.

Appendix B
RX Beamformer

The Lagrangian of the Rx beamformer problem in (5) is:

$$\mathcal{L}(\mathbf{w}^{\text{Rx}}, \lambda_1, \lambda_2) = (\mathbf{w}^{\text{Rx}})^{\text{H}}\mathbf{b}_{\text{sig}}\mathbf{b}_{\text{sig}}^{\text{H}}\mathbf{w}^{\text{Rx}} - \lambda_1((\mathbf{w}^{\text{Rx}})^{\text{H}}\mathbf{b}_{\text{SI}}\mathbf{b}_{\text{SI}}^{\text{H}}\mathbf{w}^{\text{Rx}} - \kappa_{SI}) - \lambda_2((\mathbf{w}^{\text{Rx}})^{\text{H}}\mathbf{w}^{\text{Rx}} - 1) \tag{7}$$

where λ_1 and λ_2 are Lagrange multipliers. For optimality, we set $\nabla_{(\mathbf{w}^{\text{Rx}})^{\text{H}}}\mathcal{L} = \partial_{\lambda_1}\mathcal{L} = \partial_{\lambda_2}\mathcal{L} = 0$, leading to

$$(\mathbf{b}_{\text{sig}}\mathbf{b}_{\text{sig}}^{\text{H}})\mathbf{w}^{\text{Rx}} = (\lambda_1\mathbf{b}_{\text{SI}}\mathbf{b}_{\text{SI}}^{\text{H}} + \lambda_2\mathbf{I})\mathbf{w}^{\text{Rx}} \tag{8a}$$

$$\lambda_1((\mathbf{w}^{\text{Rx}})^{\text{H}}\mathbf{b}_{\text{SI}}\mathbf{b}_{\text{SI}}^{\text{H}}\mathbf{w}^{\text{Rx}} - \kappa_{SI}) = 0, \quad \lambda_1 > 0 \tag{8b}$$

$$\lambda_2((\mathbf{w}^{\text{Rx}})^{\text{H}}\mathbf{w}^{\text{Rx}} - 1) = 0, \quad \lambda_2 > 0 \tag{8c}$$

To solve it, we iteratively increase λ_2, solve the respective eigenvalue Eq. (8a) for this constant λ_2, normalize the principal eigenvector $\mathbf{w}_{\text{opt}}^{\text{Rx}}$, repeat until $(\mathbf{w}_{\text{opt}}^{\text{Rx}})^{\text{H}}\mathbf{b}_{\text{SI}}\mathbf{b}_{\text{SI}}^{\text{H}}\mathbf{w}_{\text{opt}}^{\text{Rx}} = \kappa_{\text{SI}}$.

REFERENCES

[1] A. Sabharwal, P. Schniter, D. Guo, D. W. Bliss, S. Rangarajan, and R. Wichman, "In-band full-duplex wireless: Challenges and opportunities," *IEEE Journal on selected areas in communications*, vol. 32, no. 9, pp. 1637–1652, 2014.

[2] Z. Zhang, K. Long, A. V. Vasilakos, and L. Hanzo, "Full-duplex wireless communications: Challenges, solutions, and future research directions," *Proceedings of the IEEE*, vol. 104, no. 7, pp. 1369–1409, 2016.

[3] K. E. Kolodziej and Z. Popović, "Simultaneous-multifunction phased arrays: Enabled by in-band full-duplex technology," *IEEE Microwave Magazine*, vol. 25, no. 4, pp. 44–63, 2024.

[4] B. Smida, R. Wichman, K. E. Kolodziej, H. A. Suraweera, T. Riihonen, and A. Sabharwal, "In-band full-duplex: The physical layer," *Proceedings of the IEEE*, 2024.

[5] M. Heino, D. Korpi, T. Huusari, E. Antonio-Rodriguez, S. Venkatasubramanian, T. Riihonen, L. Anttila, C. Icheln, K. Haneda, R. Wichman *et al.*, "Recent advances in antenna design and interference cancellation algorithms for in-band full duplex relays," *IEEE Communications magazine*, vol. 53, no. 5, pp. 91–101, 2015.

[6] S. Hong, J. Brand, J. I. Choi, M. Jain, J. Mehlman, S. Katti, and P. Levis, "Applications of self-interference cancellation in 5g and beyond," *IEEE Communications Magazine*, vol. 52, no. 2, pp. 114–121, 2014.

[7] M. Mohammadi, Z. Mobini, D. Galappaththige, and C. Tellambura, "A comprehensive survey on full-duplex communication: Current solutions, future trends, and open issues," *IEEE Communications Surveys & Tutorials*, 2023.

[8] J. Beiranvand and H. Meghdadi, "Analytical performance evaluation of mrc receivers in massive mimo systems," *IEEE Access*, vol. 6, pp. 53 226–53 234, 2018.

[9] S. P. Herath and T. Le-Ngoc, "Sum-rate performance and impact of self-interference cancellation on full-duplex wireless systems," in *2013 IEEE 24th Annual International Symposium on Personal, Indoor, and Mobile Radio Communications (PIMRC)*, 2013, pp. 881–885.

[10] L. Shen, Y. Zakharov, B. Henson, N. Morozs, and P. D. Mitchell, "Adaptive filtering for full-duplex uwa systems with time-varying self-interference channel," *IEEE Access*, vol. 8, pp. 187 590–187 604, 2020.

[11] C. Mollén, U. Gustavsson, T. Eriksson, and E. G. Larsson, "Spatial characteristics of distortion radiated from antenna arrays with transceiver nonlinearities," *IEEE transactions on wireless communications*, vol. 17, no. 10, pp. 6663–6679, 2018.

[12] M. Ayebe, J. Malmström, S. E. Gunnarson, H. Holter, M. Ivashina, C. Bencivenni, and R. Maaskant, "Systematic self-interference mitigation in full duplex antenna arrays via transmit beamforming," in *2023 International Conference on Electromagnetics in Advanced Applications (ICEAA)*, 2023, pp. 158–163.

[13] K. Kurokawa, "Power waves and the scattering matrix," *IEEE transactions on microwave theory and techniques*, vol. 13, no. 2, pp. 194–202, 1965.

[14] H. L. Van Trees, *Optimum array processing: Part IV of detection, estimation, and modulation theory*. John Wiley & Sons, 2002.

[15] M. Ayebe, R. Maaskant, J. Malmström, S. E. Gunnarson, H. Holter, and M. Ivashina, "3d-printed silver-coated vivaldi array with integrated coaxial probe feeding," in *2024 IEEE International Symposium on Antennas and Propagation and INC/USNC-URSI Radio Science Meeting (AP-S/INC-USNC-URSI)*, 2024, pp. 7–8.

[16] A. Xilinx, *Zynq UltraScale+ RFSoC RF Data Converter v2.6 Gen 1/2/3/DFE*. [Online]. Available: https://docs.amd.com/r/en-US/pg269-rf-data-converter, 2022.

[17] M. Ayebe, R. Maaskant, J. Malmström, S. E. Gunnarson, H. Holter, and M. Ivashina, "Evaluation of the self-interference cancellation limits of full-duplex antenna arrays using zynq ultrascale+ rf system-on-chip board," in *2024 IEEE International Symposium on Phased Array System & Technology (PAST)*, 2024.